ADVANCED FUNCTIONAL MATERIALS
www.afm-journal.de

www.MaterialsViews.com

Voltage-Controlled Nonstoichiometry in Oxide Thin Films: $Pr_{0.1}Ce_{0.9}O_{2-\delta}$ Case Study

*Di Chen and Harry L. Tuller**

While the properties of functional oxide thin films often depend strongly on oxygen stoichiometry, there have been few means available for its control in a reliable and in situ fashion. This work describes the use of DC bias as a means of systematically controlling the stoichiometry of oxide thin films deposited onto yttria-stabilized zirconia substrates. Impedance spectroscopy is performed on the electrochemical cell $Pr_{0.1}Ce_{0.9}O_{2-\delta}$ (PCO) /YSZ/Ag for conditions: T = 550 to 700 °C, $pO_2 = 10^{-4}$ to 1 atm, and $\Delta E = -100$ to 100 mV. The DC bias ΔE is used to control the effective pO_2 or oxygen activity at the PCO/YSZ interface. The non-stoichiometry (δ) of the PCO films is calculated from the measured chemical capacitance (C_{chem}). These δ values, when plotted isothermally as a function of effective pO_2, established, either by the surrounding gas composition alone, or in combination with applied bias, agree well with each other and to predictions based on a previously determined defect model. These results confirm the suitability of using bias to precisely control δ of thin films in an in situ fashion and simultaneously monitor these changes by measurement of C_{chem}. Of further interest is the ability to reach effective pO_2s as high as 280 atm.

1. Introduction

Deviations from stoichiometry are common in transition metal and rare earth oxides and are generally associated with changes in the oxidation states of the respective cations. Well known examples include $TiO_{2-\delta}$, $Fe_{3-\delta}O_4$, $SrTi_{1-x}Fe_xO_{3-\delta}$ and $CeO_{2-\delta}$, where δ is a measure of the level of nonstoichiometry exhibited by the material under given conditions of temperature and partial pressure of oxygen, pO_2.[1–5] Many physical and chemical properties are often strong functions of δ including, for example, electrical conductivity,[6] magnetic permeability,[7] optical absorptivity and luminescence,[8] oxygen and cation diffusivities,[9] and thermal conductivity.[10,11] As an illustrative example, the room temperature electrical conductivity of $TiO_{2-\delta}$ can differ by many orders of magnitude as δ varies from near zero to ~ 0.01.[12]

Oxides, in the form of thin films, nanoparticles, or nanowires often satisfy technologically critical functions, and so are being incorporated into a rapidly growing range of devices including memristors,[13] magneto-optic based memories,[14] dye sensitized solar cells,[15] chemical sensors,[16] micro-batteries and micro-fuel cells,[17,18] just to name a few. Even with the critical role that the extent of nonstoichiometry plays in controlling the properties of these oxides, in surprisingly few cases is δ of these oxides known, or how best to control it. First, methods for measuring nonstoichiometry in situ are needed to enable one to correlate changes in δ with changes in annealing conditions. While this can be readily achieved for bulk specimens by thermogravimetric analysis (TGA) or measurement of electrical conductivity in combination with knowledge of defect mobilities,[19] it is difficult to do so in films, either because of the very small mass changes associated with thin films in the former or the potential impact of substrate-film interactions in the latter. We, and others, have had recent success in measuring nonstoichiometry of thin films by chemical capacitance and/or optical spectroscopy.[8,20–23]

In attempting to correlate film properties with oxygen nonstoichiometry, it is furthermore often difficult to experimentally access certain levels of δ, e.g., at sufficiently high temperatures or extremes in partial or total pressure of oxygen. Likewise, it is often difficult to reversibly change δ by small increments, particularly important if one is close to a phase transition or where properties are sharp functions of pO_2 as in the $VO_{2\pm\delta}$ system.[24] This requires a technique capable of precisely controlling oxygen nonstoichiometry of films in situ. While modifying δ in oxides is routinely performed by controlling the pO_2 in the gas phase, electrochemical means, by varying the bias across an electrochemical cell, offers a fast, precise and convenient alternative means for controlling oxygen stoichiometry. While some researchers have attempted to use bias to control film oxygen stoichiometry, few studies to our knowledge, have been able to simultaneously measure and control nonstoichiometry accurately. For example, Backhaus-Ricoult et al. and Chen et al. used bias to vary the oxygen stoichiometry of $La_xSr_{1-x}MnO_{3-\delta}$, but the oxygen stoichiometry itself was not measured.[25,26] Kawada et al. measured the nonstoichiometry

D. Chen, Prof. H. L. Tuller
Department of Materials Science and Engineering
Massachusetts Institute of Technology
Cambridge, MA 02139, USA
E-mail: tuller@mit.edu
Prof. H. L. Tuller
International Institute for Carbon Neutral
Energy Research (WPI-I2CNER)
Kyushu University
Nishi-ku Fukuoka 819–0395, Japan

DOI: 10.1002/adfm.201402050

of $La_{0.6}Sr_{0.4}CoO_{3-\delta}$ thin films by measurement and analysis of the chemical capacitance, C_{chem}, while varying δ under electrochemical bias, but found *it* to be much smaller in magnitude than that of bulk specimens of the same composition.[21] Furthermore, this finding was opposite to the behavior later reported by other investigators on similar compositions.[27]

In this paper, we report the ability to both monitor and control oxygen stoichiometry reversibly in $Pr_{0.1}Ce_{0.9}O_{2-\delta}$ (PCO) thin films, the latter by application of controlled DC bias in an electrochemical cell of the form Ag/YSZ/PCO. We previously reported the ability to monitor the oxygen nonstoichiometry in situ by interpretation of the measured chemical capacitance (C_{chem}) in terms of the model defining defect equilibria in PCO.[22] In this study, we apply a DC bias across the above cell, and simultaneously monitor δ by measuring C_{chem}. As we demonstrate, the δ values, at a given oxygen activity within the film, achieved with and without DC bias, agree well under all measurement conditions and fit the predictions of the defect chemical model well. This confirms the suitability of this technique for controlling the δ of oxide thin films, even under conditions difficult or impossible to achieve by conventional means, e.g., up to oxygen pressures equivalent to 280 atm.[28–30]

2. Theory

2.1. Defect Chemistry of $Pr_{0.1}Ce_{0.9}O_{2-\delta}$

A defect equilibrium model, based on the interpretation of measurements of oxygen non-stoichiometry and electrical conductivity performed on bulk $Pr_{0.1}Ce_{0.9}O_{2-\delta}$, recently published by the authors, is summarized below.[19,22] The loss of oxygen from the lattice under reducing conditions results in the introduction of doubly ionized oxygen vacancies and the reduction of Pr^{4+} to Pr^{3+}. This defect reaction, written in Kröger-Vink notation, and followed by the corresponding mass action relation, is presented in the following.

$$2Pr_{Ce}^{\times} + O_O^{\times} \leftrightarrow 2Pr_{Ce}^{'} + V_O^{\cdot\cdot} + 1/2O_2(g) \quad (1)$$

$$\frac{\left[Pr_{Ce}^{'}\right]^2\left[V_O^{\cdot\cdot}\right]pO_2^{1/2}}{\left[Pr_{Ce}^{\times}\right]^2\left[O_O^{\times}\right]} = k_{r,Pr}^{\circ}\exp\left(\frac{-\Delta H_{r,Pr}}{kT}\right) = K_{r,Pr} \quad (2)$$

where $O_O^{\times}$, $V_O^{\cdot\cdot}$, $Pr_{Ce}^{'}$, and $Pr_{Ce}^{\times}$ are oxide ions on oxygen sites, doubly positive charged (with respect to the lattice) oxygen vacancies, Pr^{3+}, and Pr^{4+}, respectively. In the equilibrium equation, $k_{r,Pr}^{\circ}$ is a pre-exponential term and $\Delta H_{r,Pr}$ is the enthalpy for the reaction.

The condition for charge neutrality is given by

$$\left[Pr_{Ce}^{'}\right] = 2\left[V_O^{\cdot\cdot}\right] \quad (3)$$

with the understanding that the concentrations of holes, reduced Ce, and oxygen interstitials are negligibly small under the experimental conditions addressed in this study. Mass and site conservation reactions are given by

$$\left[Pr_{Ce}^{'}\right] + \left[Pr_{Ce}^{\times}\right] = \left[Pr_{Ce}\right]_{total} = 0.1\left[Pr_{0.1}Ce_{0.9}O_{2-\delta}\right] \quad (4)$$

$$\left[V_O^{\cdot\cdot}\right] + \left[O_O^{\times}\right] = 2\left[Pr_{0.1}Ce_{0.9}O_{2-\delta}\right] \quad (5)$$

where $\left[Pr_{0.1}Ce_{0.9}O_{2-\delta}\right]$ is the concentration of PCO in #/cm^{-3}. Additionally, the enthalpy of reduction of both undoped and Pr doped ceria have been reported to vary linearly with non-stoichiometry (δ), which for the case of PCO, is: [19,31]

$$\Delta H_{r,Pr} = \Delta H_{r,Pr}^{\circ} + f\delta \quad (6)$$

with $\delta = \left[V_O^{\cdot\cdot}\right]/\left[Pr\,0.1Ce_{0.9}O_2\right]$, and f is a coefficient which takes into account variations in the enthalpy change with change in stoichiometry.

2.2. Oxygen Nonstoichiometry (δ) Extracted from C_{chem}

In an MIEC electrode such as PCO, three key rate-limiting processes need to be considered for oxygen transport from the gas phase into the dense electrode and ultimately into the electrolyte. These are (i) oxygen surface exchange at the electrode-gas interface, (ii) mass transport through the electrode, and (iii) transfer of oxygen ions across the PCO/YSZ interface, as shown in **Figure 1**(a). In our previous work, we demonstrated that the surface reaction is the limiting step.[32] In this case, when a small DC bias ΔE is applied across the electrolyte, the effective oxygen potential at the electrode/electrolyte interface becomes $ze\Delta E$ relative to that in the gas phase, for which the net charge transferred, z, per O_2, equals 4 and e is the charge of an electron. This results in an oxygen potential profile at the film/gas interface as shown in Figure 1(b).[21,33]

Following the approach taken by Kawada et al.,[21] one begins by noting that the oxygen potential in the electrode $\mu_{O_2,eff}$ is related to that in the gas phase $\mu_{O_2,g}$ by

$$\mu_{O_2,eff} = \mu_{O_2,g} + 4e\Delta E \quad (7)$$

The effective oxygen partial pressure in the electrode can therefore be written as

$$pO_{2,eff} = pO_{2,g}\exp\left(\frac{4e\Delta E}{kT}\right) \quad (8)$$

The chemical capacitance (C_{chem}) is a measure of the chemical storage capacity of a material under an applied potential,[20,21] in this case reflected in the formation/annihilation of $V_O^{\cdot\cdot}$ and $Pr_{Ce}^{'}$.

$$C_{chem} = -\frac{8e^2V_{film}}{kT}\left(pO_2\frac{\partial\left[V_O^{\cdot\cdot}\right]}{\partial pO_2}\right) \quad (9)$$

in which V_{film} is the film volume, and all other terms have their familiar meaning. Substituting pO_2 by $pO_{2,eff}$, C_{chem} is expressed as:

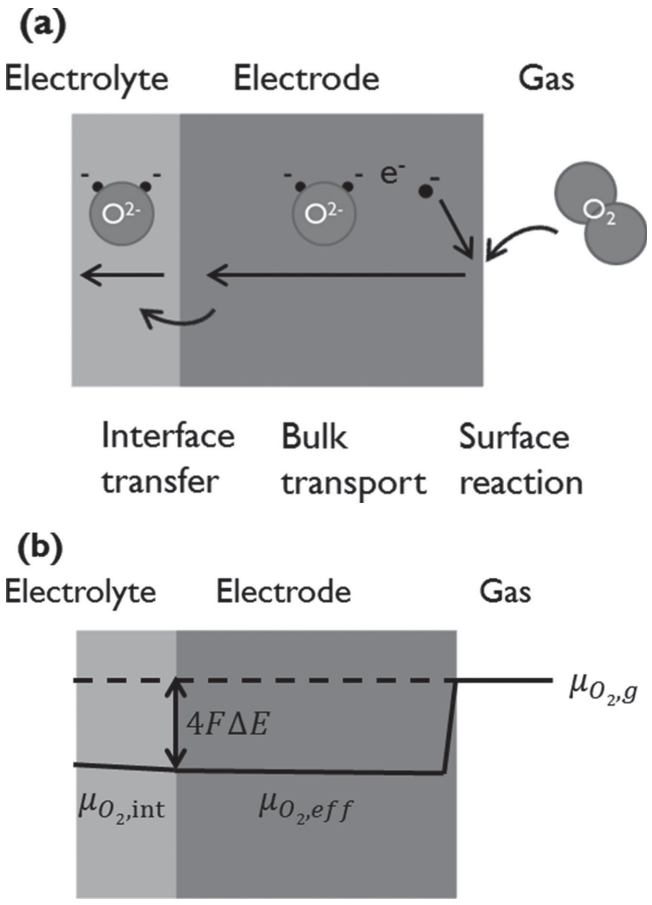

Figure 1. a) Typical limiting reaction paths for oxygen reduction on MIEC electrodes. b) Corresponding oxygen potential profile at a dense electrode when a small voltage perturbation ΔE is applied to the electrode. Consistent with this study, bulk transport and interface transfer are assumed to be fast, so there is no potential drop in the electrode nor at the electrode/electrolyte interface. Figure modified, with permission.[21] Copyright 2002, The Electrochemical Society.

$$C_{chem} = -\frac{8e^2 V_{film}}{kT}\left(pO_{2,eff}\frac{\partial\left[\mathrm{V_O^{\cdot\cdot}}\right]}{\partial pO_{2,eff}}\right) \tag{10}$$

The oxygen concentration can be estimated at each $pO_{2,eff}$ through integration of Equation (10) with respect to $pO^{\circ}_{2,eff}$ as

$$\left[\mathrm{V_O^{\cdot\cdot}}\right]\left(pO_{2,eff}\right) = \frac{kT}{8e^2 V_{film}}\int_{chem}^{C} d\ln pO_{2,eff} + \left[\mathrm{V_O^{\cdot\cdot}}\right]\left(pO^{\circ}_{2,eff}\right) \tag{11}$$

where $pO^{\circ}_{2,eff}$ is a reference oxygen pressure at which $\left[\mathrm{V_O^{\cdot\cdot}}\right]$ is known.

In the case of the PCO system, the ability to extract reliable reference values for $\left[\mathrm{V_O^{\cdot\cdot}}\right]\left(pO^{\circ}_{2,eff}\right)$ directly from measurements of C_{chem} has been demonstrated by our group.[22] In the high pO_2 region, C_{chem} is given by

$$C_{chem} = \frac{4}{3}\frac{e^2 V_{film}}{kT}\left[\mathrm{V_O^{\cdot\cdot}}\right] \tag{12}$$

Values of δ at other pO_2 region were calculated by using Equation (11) utilizing the reference values obtained with Equation (12).

3. Results

3.1. Film Characterization

The XRD pattern obtained from 2θ-ω coupled scans of the YSZ single crystal, with and without the PCO film, exhibited only (001) fluorite peaks, demonstrating that the PLD deposited PCO films were fluorite structured with a highly (001) oriented texture. Surface analysis by AFM showed a dense and smooth film with apparent grain size of approximately 50 nm and surface roughness of approximately 0.5 nm. Details of film characterization are discussed elsewhere.[32]

3.2. EIS Spectra and Equivalent Circuit

Figure 2 shows typical impedance spectra obtained. As shown in the inset, the spectra are all represented by a resistor in series with an R//Q circuit (R//Q: a resistor in parallel with a constant phase element [CPE]). CPEs are used to take into account any inhomogeneities in the electrodes resulting in "depressed" arcs not well represented by ideal capacitors.[34] The impedance of a CPE is given by

$$Z = \frac{1}{Q(i\omega)^{n_q}} \tag{13}$$

where ω, i, and n_q are angular frequency, $\sqrt{-1}$, and a factor related to the deviation from ideal capacitance, respectively. An equivalent capacitance is derived from Q using the following equation[35]

$$C = Q\omega_{max}^{n_q-1} = \left(R^{1-n_q}Q\right)^{1/n_q} \tag{14}$$

The equivalent circuit fits are observed to represent the data well. The origin of each component is discussed in the authors' previous work.[22,32] R_{YSZ} reflects the series YSZ Ohmic contribution to the overall cell impedance, and R_{PCO} is the electrode resistance at the PCO/gas interface, limited by oxygen surface exchange kinetics. C_{PCO} is the chemical capacitance of the PCO film. Since there is a reference electrode on the YSZ substrate, there is no contribution from the porous Ag electrode apparent in the impedance spectra. Typical n_q values near unity (0.93 – 1.04 measured) for Q corresponding to C_{PCO} (see Equation (14)) demonstrate near ideal capacitance.

3.3. Bias Dependence of C_{chem}

Figure 3 summarizes C_{chem} values measured at four different pO_2s (1, 10^{-1}, 10^{-2} and 10^{-3} atm) with either zero bias or with applied voltages, ΔE *of* ± 25, ± 50 and ± 100 mV. Several clear trends are observed. At zero bias, C_{chem} increases with decreasing pO_2 at 550 °C but becomes systematically less sensitive to pO_2 at

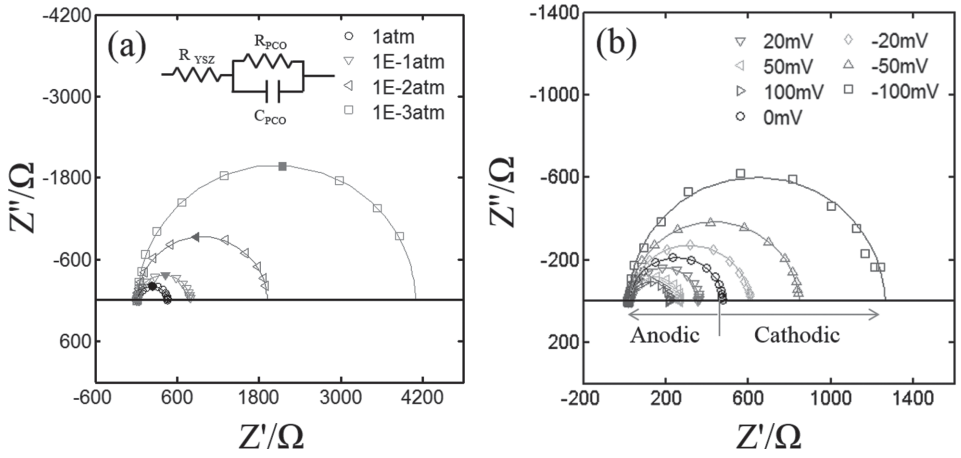

Figure 2. a) Typical impedance spectra collected at 650 °C, 0 mV DC bias, at various oxygen partial pressures as indicated. The filled symbols shows the impedance at peak frequencies, f = 0.202 Hz, 0.080 Hz, 0.032 Hz, 0.013 Hz, respectively, from low pO_2 to high pO_2. The inset shows the equivalent circuit used to fit the data. b) Typical impedance spectra collected at 650 °C, 1 atm pO_2, at various DC biases, as indicated. Both impedance spectra in (a) and (b) are obtained from a symmetric PCO/YSZ/Ag cell with PCO film thickness of 58 nm with symbols representing the experimental data while the solid lines are the equivalent circuit fit.

the lower pO_2 end, as temperature increases. This is consistent with what was observed in our previous studies.[22] A generally strong dependence of C_{chem} on bias, at a given atmosphere, is observed at 550 °C, with C_{chem} increasing with negative bias and decreasing with positive bias. This dependence becomes weaker as temperature is increased, particularly for negative bias conditions. Indeed, at each pO_2, C_{chem} passes through a maximum, with the maximum moving towards less negative bias conditions as the temperature increases.

4. Discussion

4.1. Effective pO_2 Dependence of C_{chem}

In **Figure 4**, the C_{chem} data shown in Figure 3 are replotted, at each temperature, as a function of $pO_{2,eff}$ in which ΔE was converted to values of $pO_{2,eff}$ with the aid of Equation (8). The filled symbols represent the capacitance measured in equilibrium with the gas phase, i.e., $\Delta E = 0$, while the empty symbols represent data obtained under an applied bias, ΔE. All the isotherms exhibit a maximum, with the maximum shifting to increasing pO_2 with increasing temperature, as observed in previous studies in which C_{chem} was measured without applied bias.[22] Returning to the definition of C_{chem} given in Equation (9), this maximum simply corresponds to the condition at which the rate of change in oxygen vacancy concentration or δ with change in pO_2 is at its peak. Also included in the figure, as a solid curve, are calculated values of C_{chem} derived from the previously determined defect equilibrium model which provides for the prediction of $\left[V_O^{\cdot\cdot}\right]$ as functions of temperature and pO_2. One observes a generally good fit between the predicted and measured values of C_{chem} whether obtained with or without bias.

4.2. Non-Stoichiometry Dependence on $pO_{2,eff}$

Figure 5 shows the δ values extracted from C_{chem}, derived with the aid of Equation (11) and (12), as a function of $pO_{2,eff}$ for

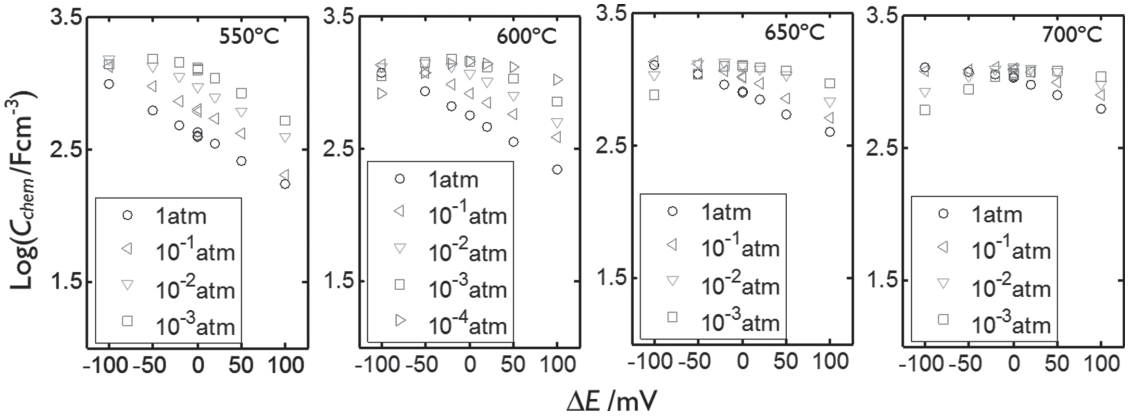

Figure 3. Chemical capacitance as a function of applied voltage at various oxygen partial pressures, as indicated.

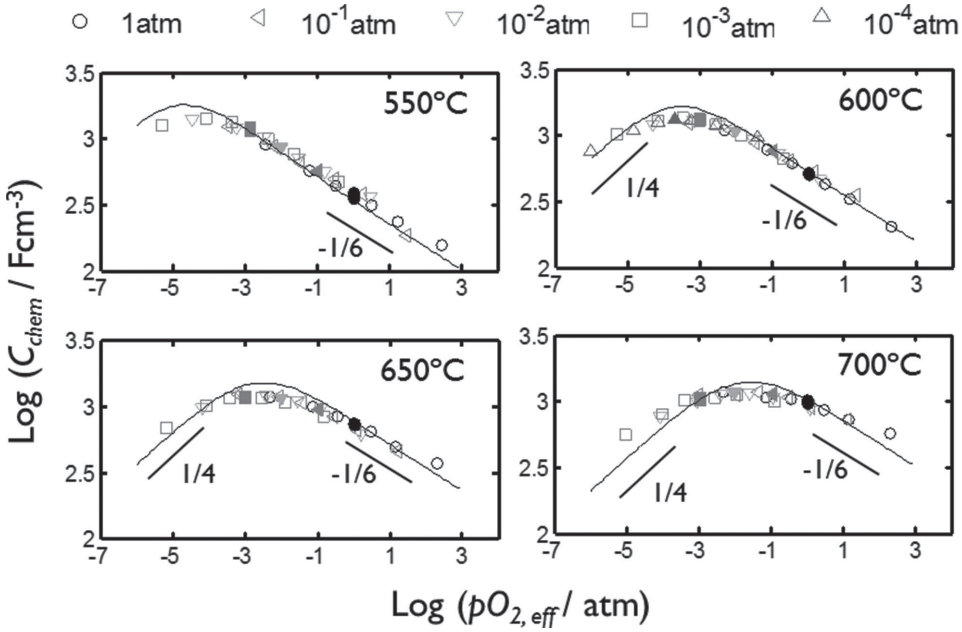

Figure 4. Isothermal dependence of volume-specific C_{chem} (symbols) on pO_2, obtained from a PCO/YSZ/Ag cell with PCO film thickness of 58 nm. The filled symbols indicate capacitances under zero bias. The empty symbols indicate capacitances measured with bias applied. Solid lines represent modeled data.

a series of isotherms ranging from 550 to 700 °C. The results are compared to δ values with parameters listed in **Table 1** (dash lines). First, one observes excellent registry and little scatter between δ values derived from C_{chem} with and without DC bias. This points to the effectiveness of bias in controlling non-stoichiometry in PCO. Second, δ values extracted from C_{chem} match well with those predicted from the defect model as reported previously based on data limited to the high partial pressures of oxygen (10^{-5} to 1 atm).[22] Note, in both studies, the magnitude of the enthalpy of reduction, $H_{r,Pr}$ is lower in the film than in the bulk, pointing to the more ready reduction of the film than that of the bulk. The only significant deviation of the data from the predicted model occurs at the lowest isotherm of 550 °C, wherein the experimental data show a somewhat steeper dependence on pO_2. This may reflect the greater difficulty in reaching equilibrium at lower temperatures.[32] These results confirm the suitability of using bias across an electrochemical cell to conveniently and precisely control δ of oxide thin films in an in situ fashion and simultaneously monitor these changes by measurement of the chemical capacitance.

Table 1. Parameters used in the defect equilibrium model for $Pr_{0.1}Ce_{0.9}O_{2-\delta}$ (see Equations (2) and (6) for definition of parameters). The parameters for thin films are determined by C_{chem}, while the parameters for bulk are determined by TGA. $[Pr_{0.1}Ce_{0.9}O_{2-\delta}] = 2.52 \times 10^{22}$ cm^{-3} for density = 7.21g·cm^{-3}.[19]

Morphology	$\Delta H^{\circ}_{r,Pr}$, [eV]	$k^{\circ}_{r,Pr}$, [atm$^{1/2}$]	f, [eVδ^{-1}]
Thin film (This work)	1.79 ± 0.03	(1.2 ± 0.3) × 10^6	−4.5 ± 1.0
Thin film (Previous work)[22]	1.80 ± 0.04	(0.9 ± 0.6) × 10^6	−6.2 ± 1.5
Bulk[19]	1.90 ± 0.07	(2.1 ± 1.2) × 10^6	−4.63 ± 1.9

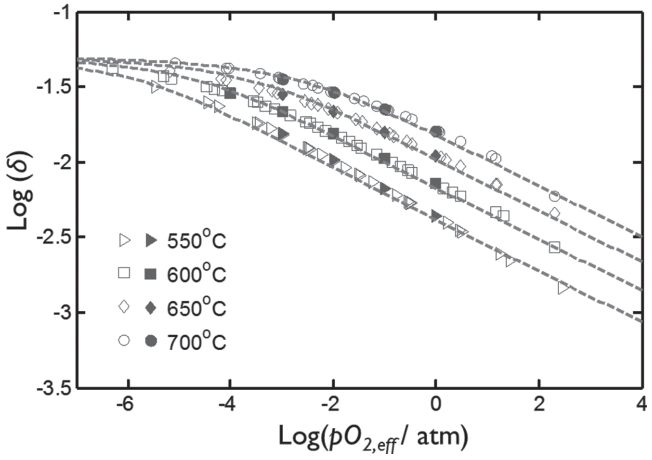

Figure 5. Isothermal dependence of non-stoichiometry (symbols) on $pO_{2,eff}$ calculated from C_{chem} in Figure 4. The filled symbols represent non-stoichiometry values obtained for zero bias while empty symbols represent those obtained with bias applied. Dash lines represent modeled data.

A potentially highly attractive feature in utilizing bias to access higher and lower oxygen activities than those existing in the surrounding gas phase is the possibility of reaching oxygen acitivities otherwise very difficult to achieve experimentally. Specifically, in this study one observes in Figures 4 and 5, that values of $pO_{2,eff}$ as high as 280 atm were reached by application of a positive bias of 100 mV without need for more complex high pressure apparatus, as used in previous studies.[28–30] Interestingly, the data collected for $pO_{2,eff}$ values above 1 atm continue to fit the predicted model quite well, even though, at

these high oxygen activities, one would expect to have to replace defect concentrations with activities.

As discussed in the introduction, many properties of oxides are strong functions of δ. By control of δ by DC bias, these properties can then, in principle, be tuned precisely and over wide limits. Possible applications could be to memristors, transparent conducting oxide electrodes, thermoelectrics, etc.

While ultrahigh-vacuum (UHV) surface science, introduced in the 1960s, provides insight into the adsorption processes, only recently have modern techniques enabled experiments to be conducted under near ambient pressure, such as Ambient-Pressure X-ray Photoelectron Spectroscopy (AP-XPS),[36] high-pressure scanning tunneling microscopy (HP-STM),[37] Reflection high-energy electron diffraction (RHEED),[38] TEM, SEM, etc. In these studies, either differential pumping is used to maintain the detector at higher pressures, or an electron transparent membrane is used to seal the sample inside the specimen chamber in which the atmosphere can be controlled to some degree. With the arrangement demonstrated in this study, it may be possible to conveniently vary and control the film δ within such instrument chambers.

5. Conclusion

The nonstoichiometry (δ) of a $Pr_{0.1}Ce_{0.9}O_{2-\delta}$ thin film was systematically controlled by application of a DC bias across an electrochemical cell of the form Ag/YSZ/PCO for the temperature and pO_2 ranges of $550 \le T \le 700$ °C and $10^{-4} \le pO_2 \le 1$ atm, respectively. δ values derived from an analysis of the chemical capancitance (C_{chem}) data agree well with values prediced from a previously determined defect chemical model. This confirms the suitability of the application of bias as a means of conveniently and accurately controlling δ of oxide thin films even to $pO_{2,eff}$ values considerably above 1 atm. This technique offers a number of key advantages for modifying δ in films:

- High precision: Bias control offers much higher precision in controlling the oxygen activity in the film than by the common method of mixing of appropriate gases with the aid of MFCs (mass flow controllers). Bias control enables one to modify oxygen activity in very small increments, thereby offering the ability to study the pO_2 dependence of various properties within a narrow $pO_{2,eff}$ range. This is particurlaly useful when wishing to study materials with very narrow phase fields, such as those in the vanadium-oxygen system.
- Wider oxygen activity range: Bias control could be used to study the defect chemistry of an oxide at high oxygen activity (up to 280 atm) or within instrument vacuum chambers, otherwise experimentally difficult to achieve.
- Faster: Electrochemical control bypasses the need for films to equilibrate via gas surface exchange, thereby markedly accelerating the time needed to achieve a new steady or equilibrium state of the film.

5. Experimental Section

Sample Preparation and Characterization: Details of $Pr_{0.1}Ce_{0.9}O_{2-\delta}$ film preparation were discussed elsewhere;[32] a summary is given here. Films were deposited onto (001) oriented single crystal YSZ (8 mol% Y_2O_3 stabilized) substrates ($5 \times 10 \times 0.5$ mm^3; MTI Corporation, Richmond, CA) by pulsed laser deposition (PLD) from oxide targets. The film structure was analyzed by X-ray diffraction (XRD; X'Pert PRO MPD, PANalytical) with approximate grain size and surface roughness determined by atomic force microscopy (Digital Instruments Nanoscope IIIa) and film thickness determined by surface profilometry (KLA-Tencor P-16+ stylus profiler).

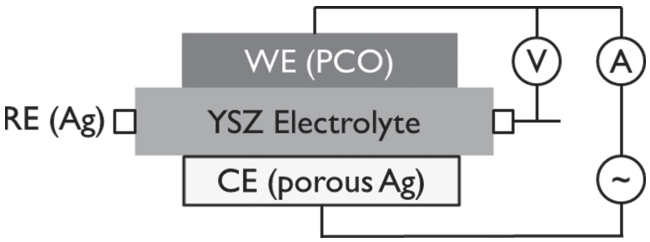

Figure 6. Geometry of the working (WE), reference (RE), and counter (CE) electrode for the impedance measurement.

Electrical and Electrochemical Measurements: An asymmetrical cell, as illustrated in **Figure 6** was used for the measurements. Identically sized (5×9 mm^2) PCO working electrode and porous Ag counter electrode (SPI Silver Paste Plus, SPI Supplies, Chester, PA, USA) were applied to opposite sides of a single crystal YSZ substrate/electrolyte. The same Ag paste was applied to the edge of the YSZ substrate as the reference electrode. Au paste (Fuel cell materials, Lewis Center, Ohio), serving as current collector, was applied to the top surface of the PCO electrode. The electrochemical impedance measurements were performed at temperatures between 550 and 700 °C and oxygen partial pressures between 10^{-4} and 1 atm, controlled by mixing N_2 and O_2 with the aid of mass flow controllers (MKS) and monitored by an in situ YSZ Nernst type oxygen sensor. IS measurements, covering the frequency range from 0.032 Hz to 1 MHz, with AC amplitude of 10 mV, DC bias range of $\Delta E = -100$ mV to 100 mV, were performed using an impedance analyzer (Solartron 1260) with data fit to equivalent circuits using Zview and Zplot software (Scribner Associates).

Data Fitting: Data fitting to defect models to obtain thermodynamic parameters was performed using Matlab (Mathworks). Parameters in the models were determined using the Gauss-Newton method of non-linear regression with partial derivatives approximated numerically.[39] Initial estimations were refined visually and then regression was performed in a step-wise iterative manner. Error estimates for modeled parameters are reported for an approximate 95% confidence interval of the regressed model.

Acknowledgements

This work was supported by the Basic Energy Sciences, U.S. Department of Energy under award DE-SC0002633. The authors thank Jae Jin Kim (MIT) for preparation of the PLD targets.

Received: June 20, 2014
Revised: September 6, 2014
Published online: October 9, 2014

[1] M. K. Nowotny, T. Bak, J. Nowotny, *J. Phys. Chem. B* **2006**, *110*, 16270.
[2] F. C. Voogt, T. Hibma, G. L. Zhang, M. Hoefman, L. Niesen, *Surf. Sci.* **1995**, *331–333*, 1508.
[3] A. Rothschild, W. Menesklou, H. L. Tuller, E. Ivers-Tiffée, *Chem. Mater.* **2006**, *18*, 3651.
[4] H. L. Tuller, *J. Electrochem. Soc.* **1979**, *126*, 209.
[5] J. Engel, S. R. Bishop, L. Vayssieres, H. L. Tuller, *Adv. Funct. Mater.* **2014**, DOI: 10.1002/adfm.201400203.
[6] H. L. Tuller, S. R. Bishop, *Annu. Rev. Mater. Res.* **2011**, *41*, 369.

[7] H. S. Hsu, J. C. A. Huang, Y. H. Huang, Y. F. Liao, M. Z. Lin, C. H. Lee, J. F. Lee, S. F. Chen, L. Y. Lai, C. P. Liu, *Appl. Phys. Lett.* **2006**, *88*, 242507.
[8] J. J. Kim, S. R. Bishop, N. Thompson, D. Chen, H. L. Tuller, *Chem. Mater.* **2014**, *26*, 1374.
[9] E. Boehm, J. Bassat, P. Dordor, F. Mauvy, J. Grenier, P. Stevens, *Solid State Ionics* **2005**, *176*, 2717.
[10] C. Yu, M. L. Scullin, M. Huijben, R. Ramesh, A. Majumdar, *Appl. Phys. Lett.* **2008**, *92*, 191911.
[11] M. N. Luckyanova, D. Chen, W. Ma, H. L. Tuller, G. Chen, B. Yildiz, *Appl. Phys. Lett.* **2014**, *104*, 061911.
[12] Y. Lu, K. Sagara, L. Hao, Z. Ji, H. Yoshida, *Mater. Trans.* **2012**, *53*, 1208.
[13] D. B. Strukov, G. S. Snider, D. R. Stewart, R. S. Williams, *Nature* **2008**, *453*, 80.
[14] J.-P. Krumme, *Appl. Phys. Lett.* **1973**, *23*, 576.
[15] A. Hagfeldt, G. Boschloo, L. Sun, L. Kloo, H. Pettersson, *Chem. Rev.* **2010**, *110*, 6595.
[16] Y. Min, H. L. Tuller, S. Palzer, J. Wöllenstein, H. Böttner, *Sens. Actuators B Chem.* **2003**, *93*, 435.
[17] C. Branci, N. Benjelloun, J. Sarradin, M. Ribes, *Solid State Ionics* **2000**, *135*, 169.
[18] M. Tsuchiya, B.-K. Lai, S. Ramanathan, *Nat. Nanotechnol.* **2011**, *6*, 282.
[19] S. R. Bishop, T. S. Stefanik, H. L. Tuller, *Phys. Chem. Chem. Phys.* **2011**, *13*, 10165.
[20] W. C. Chueh, S. M. Haile, *Phys. Chem. Chem. Phys.* **2009**, *11*, 8144.
[21] T. Kawada, J. Suzuki, M. Sase, A. Kaimai, K. Yashiro, Y. Nigara, J. Mizusaki, K. Kawamura, H. Yugami, *J. Electrochem. Soc.* **2002**, *149*, E252.
[22] D. Chen, S. R. Bishop, H. L. Tuller, *Adv. Funct. Mater.* **2013**, *23*, 2168.
[23] D. Chen, S. R. Bishop, H. L. Tuller, *ECS Trans.* **2013**, *57*, 1387.
[24] N. F. Mott, L. Friedman, *Philos. Mag.* **1974**, *30*, 389.
[25] M. Backhaus-Ricoult, K. Adib, T. S. Clair, B. Luerssen, L. Gregoratti, A. Barinov, *Solid State Ionics* **2008**, *179*, 891.
[26] X. J. Chen, S. H. Chan, K. A. Khor, *Electrochem. Solid-State Lett.* **2004**, *7*, A144.
[27] G. J. la O', S.-J. Ahn, E. Crumlin, Y. Orikasa, M. D. Biegalski, H. M. Christen, Y. Shao-Horn, *Angew. Chem. Int. Ed. Engl.* **2010**, *49*, 5344.
[28] E. Baker, M. Iqbal, B. Knox, *J. Mater. Sci.* **1977**, *12*.
[29] H. Takamura, J. Kobayashi, N. Takahashi, M. Okada, *J. Electroceramics* **2008**, *22*, 24.
[30] R. Waser, *J. Am. Ceram. Soc.* **1991**, *40*, 1934.
[31] C. Chatzichristodoulou, P. V. Hendriksen, A. Hagen, *J. Electrochem. Soc.* **2010**, *157*, B299.
[32] D. Chen, S. R. Bishop, H. L. Tuller, *J. Electroceramics* **2012**, *28*, 62.
[33] W. C. Chueh, S. M. Haile, *Annu. Rev. Chem. Biomol. Eng.* **2012**, *3*, 313.
[34] S. B. Adler, *Chem. Rev.* **2004**, *104*, 4791.
[35] J. Fleig, *Solid State Ionics* **2002**, *150*, 181.
[36] W. C. Chueh, A. H. McDaniel, M. E. Grass, Y. Hao, N. Jabeen, Z. Liu, S. M. Haile, K. F. McCarty, H. Bluhm, F. El Gabaly, *Chem. Mater.* **2012**, *24*, 1876.
[37] J. A. Jensen, K. B. Rider, M. Salmeron, G. A. Somorjai, *Phys. Rev. Lett.* **1998**, *80*, 1228.
[38] G. J. H. M. Rijnders, G. Koster, D. H. a. Blank, H. Rogalla, *Appl. Phys. Lett.* **1997**, *70*, 1888.
[39] S. Chapra, R. Canale, *Numerical Methods for Engineers*, McGraw-Hill, Inc., **2005**.